**Biogeosciences
Discussions**

Plankton ecosystem functioning and nitrogen fluxes in the most oligotrophic waters of the Beaufort Sea, Arctic Ocean: a modeling study

V. Le Fouest[1], B. Zakardjian[2], H. Xie[3], P. Raimbault[4], F. Joux[5], and M. Babin[6]

[1]Laboratoire d'Océanographie de Villefranche, BP 8, CNRS, UMR7093, Université Pierre et Marie Curie, 06238 Villefranche-sur-Mer Cedex, France
[2]Mediterranean Institute of Oceanography, Laboratoire de Sondages Électromagnétiques de l'Environnement Terrestre (LSEET-LEPI), Université de Toulon et du Var, 83957 La Garde Cedex, France
[3]Institut des sciences de la mer de Rimouski, Université du Québec à Rimouski, 310, allée des Ursulines, C.P. 3300 Rimouski (Québec) G5L 3A1, Canada
[4]Mediterranean Institute of Oceanography, Institut Méditerranéen d'Océanologie, OSU Pythéas, Campus de Luminy, 13288 Marseille, France
[5]Laboratoire d'Océanographie Microbienne, CNRS UMR 7621 & Université Pierre et Marie Curie, 66650 Banyuls-sur-Mer, France

[6]Takuvik Joint International Laboratory, Université Laval (Canada) & Centre National de la Recherche Scientifique (France), Département de Biologie, 1045, Avenue de la Médecine, Québec (Québec), G1V 0A6, Canada

Correspondence to: V. Le Fouest (lefouest@obs-vlfr.fr)

Abstract

The Arctic Ocean (AO) undergoes profound changes of its physical and biotic environments due to climate change. The greater light exposure and stratification alter its plankton ecosystem structure, functioning and productivity promoting oligotrophy in some areas as the Beaufort Sea. A one-dimension (1-D) physical-biological coupled model based on the large multiparametric database of the Malina project in the Beaufort Sea was used (i) to infer the functioning and nitrogen fluxes within the summer plankton ecosystem and (ii) to assess the model sensitivity to key light-associated processes involved in nutrient recycling and phytoplankton growth. The coupled model suggested that ammonium photochemically produced from photosensitive dissolved organic nitrogen (i.e. photoammonification process) was a necessary nitrogen source to achieve the observed levels of microbial biomass and production. It contributed to ca. two-thirds and one-third of the simulated surface (0–10 m) and depth-integrated primary and bacterial production, respectively. The model also suggested that carbon to chlorophyll ratios for small ($< 5\,\mu m$) phytoplankton (ca. 15–$45\,\mathrm{g\,g^{-1}}$) lower than those commonly used in biogeochemical models applied to the AO were required to simulate the observed herbivorous versus microbial food web competition and realistic nitrogen fluxes in the Beaufort Sea oligotrophic waters. In face of accelerating Arctic warming, more attention should be paid in the future to the mechanistic processes involved in food webs and functional groups competition, nutrient recycling and primary production in poorly productive waters of the AO as they are expected to expand rapidly.

1 Introduction

The Arctic Ocean (AO) undergoes profound changes of its physical and biotic environments due to climate change. Overall net primary production (PP) is shown to have increased in the last decades (Bélanger et al., 2012; Arrigo et al., 2011) and is expected to follow this trend in the future (Slagstad et al., 2011). Nevertheless, the PP

response is not same everywhere in the AO with regions showing stable or even decreasing PP (Arrigo et al., 2011; Slagstad et al., 2011). The greater light exposure and stratification of the water column also results in earlier spring blooms (Kahru et al., 2011) and a growing contribution of small phytoplankton cells to the planktonic community in summer (Li et al., 2009) suggesting oligotrophy is expanding in some Arctic regions. Furthermore, the 40 % projected widening of the productive time period will probably allow heterotrophic organisms to optimize grazing on phytoplankton and hence alter the carbon quality and quantity exported to the benthic realm (Wassmann and Reigstad, 2011). In this context of accelerating Arctic warming, a better knowledge of the mechanistic processes and biogenic fluxes mediating PP is required, with a particular attention to the oligotrophic season when biogenic fluxes are complex and so far are poorly quantified.

In the AO, more than 80 % of the PP takes place in shelf seas (Sakshaug, 2004). The Beaufort Sea exhibits the lowest production rate (8 Tg C; Sakshaug, 2004) with respect to its surface area (ca. 476 000 km^2), which makes it the most oligotrophic shelf sea in summer (Ardyna et al., 2012). After the bloom occurring in June, a deep chlorophyll (Chl) maximum (DCM) forms as a result of relatively low nitrate concentrations in the surface layer at the end of spring (Tremblay et al., 2008). Over the growth season, the DCM progressively lowers the nitracline down to 60 m depth, where light becomes the limiting factor (Martin et al., 2010). On the slope of the Mackenzie Shelf, where the most oligotrophic waters were found (Tremblay et al., 2012), picoplankton (Micromonas ecotype) and phytoplankton < 5 µm dominated respectively the surface and DCM autotrophic community (Balzano et al., 2012; Claustre and Ras, unpublished data) whose role is central in mediating carbon fluxes in summer (Li et al., 2009).

The ability of ecosystem models applied to the AO to simulate realistic summer plankton dynamics and production rates is generally poor (e.g. Le Fouest et al., 2011). It is mostly due to a simplistic representation of key processes partly resulting from the lack of joint multiparametric measurements, especially nutrients turnover rates and light-related parameters. Such measurements were done in the Beaufort Sea during

the Malina project (http://malina.obs-vlfr.fr) in summer 2009 providing an opportunity to improve plankton ecosystem models. A physical-biological coupled model of the water column was set up based on the extensive use of physical and biogeochemical variables and rates measured during the Malina cruise. Steady state runs were

5 analyzed to budget the system and to gain a better understanding of the plankton ecosystem functioning in the most oligotrophic shelf waters of the AO. The objectives of this study are, on one hand, to infer the functioning and nitrogen fluxes within the summer plankton ecosystem and, on the other hand, to assess the model sensitivity to key light-associated processes involved in nutrient recycling and phytoplankton growth.

10 2   Material and methods

2.1   Observations

The large multiparametric dataset of physical, chemical and biological measurements collected during the Malina cruise (18 July–24 August, 2009) in the Beaufort Sea was used (i) to initiate and constrain the model runs, (ii) to set parameters and transfer

15 functions and (iii) to compare with the model outputs. We provide here a summary of the data used along with their respective reference in the Malina special issue, where the detailed methodology for each measurement can be found. Temperature, salinity and fluorescence were measured using a Conductivity-Temperature-Depth (CTD) sensor. Temperature and salinity data were used to compute potential density, which were

20 in turn used to compute Brunt-Väisälä frequencies (N). The latter were calculated in a leap-frog fashion, with the potential density from the previous and following depths (i.e. N at 5 m is computed with the data at 4 m and 6 m) (Gratton and Prieur, unpublished data). Surface and vertical profiles of downwelling photosynthetic available radiation (PAR) were respectively measured by an on-deck sensor and a Compact-Optical

25 Profiling System (C-OPS) profiler (Hooker et al., 2012). With respect to photosynthesis parameters, initial slopes (α) and light saturation parameters (E_k) were taken from Huot

Arctic plankton modeling

V. Le Fouest et al.

Discussion Paper | Discussion Paper | Discussion Paper | Discussion Paper

et al. (2012). Ammonium concentrations (NH_4) were determined on board by fluorometer according to Holmes et al. (1999). Nitrate concentrations (NO_3) were quantified at laboratory using an automatic colorimetric procedure (Raimbault et al., 1990). Rates of primary production, NH_4 and NO_3 uptake, and NH_4 regeneration and nitrification were measured using a dual $^{13}C/^{15}N$ isotopic technique (Raimbault et al., 1999) applied during 24 h in-situ incubation. Size-fractionated Chl concentrations measured during the Malina cruise following the methodology described in Ardyna et al. (2011) were used (Bélanger, unpublished data). Particulate organic carbon (POC) measurements (Doxaran et al., 2012) were used to compute POC : Chl ratios. Bacterial biomasses were derived from the product of the measured cell counts with the measured mean carbon content per cell (15.2 fg; Ortega-Retuerta et al., 2012a). Production rates estimated in $pmol\,Leu\,l^{-1}\,h^{-1}$ were converted into carbon equivalent using a conversion factor of $1.5\,kg\,C\,(mol\,Leu)^{-1}$ (Kirchman et al., 2009). Copepods biomasses were obtained from underwater video profiler data converted into carbon unit (Forest et al., 2012) and then into nitrogen using a molar C : N ratio of 8.1 (Forest et al., 2010).

2.2 The coupled physical-biological model

Based on the Malina cruise dataset, a mass-based ($mmol\,N\,m^{-3}$) plankton ecosystem model was coupled to a vertically-resolved one-dimension (1-D) physical model to compute biogeochemical concentrations and fluxes at the slope and ice-edge station 345 sampled on 14–16 August, 2009 (Fig. 1). This station was chosen with regard to the very oligotrophic conditions observed and the extensive multiparametric dataset available. The coupled model extends vertically to 200 m deep with constant 1 m layers. It is constrained by a stationary field of vertical diffusion coefficient (K_z, $m^2\,d^{-1}$) and a diurnal cycle of surface PAR (E_0, $Ein\,m^{-2}\,d^{-1}$). K_z was computed from a mean Brunt-Väisälä (N) profile derived from measurements collected in 14–16 August and turbulent kinetic energy turbulent dissipation rates ($\varepsilon = 5 \times 10^{-8}$ to $5 \times 10^{-7}\,m^2\,s^{-3}$) using the Osborn (1980) formulation ($K_z = 0.25\frac{\varepsilon}{N^2}$). A diurnal cycle of E_0 was obtained

by fitting a cosine function to E_0 on-deck measurements (14–15 August) at the same station. Both physical forcing fields are shown in Fig. 2.

The plankton ecosystem model (Fig. 3) fully detailed in the appendix is of moderate complexity and includes 10 compartments chosen according to the ecosystem structure observed during the cruise and measurements available. Phytoplankton is size-fractionated into large ($> 5 \, \mu m$) and small ($< 5 \, \mu m$) phytoplankton (LP and SP, respectively). The two zooplankton compartments represent large (LZ, mainly copepods) and small (SZ, protozooplankton) organisms. Bacteria are explicitly represented following the model of Fasham et al. (1990). Available nutrients for phytoplankton growth are nitrate (NO_3) and ammonium (NH_4). Detrital (i.e. produced by the ecosystem model compartments) particulate and dissolved organic nitrogen (PON and DONl, respectively) close the nitrogen cycle. The standing stock of potentially photosensitive DON (DONp) is photochemically transformed into NH_4 within the first 10 m of the water column. LP and SP growth depends on light, NO_3 and NH_4 availability according to the Liebig's law of minimum. LZ graze on LP and SZ, whereas SZ graze on SP and bacteria. Fecal pellets and LP basal mortality fuel the detrital PON pool. The detrital DONl pool is made of unassimilated nitrogen resulting from SZ grazing, SP and SZ basal mortality and detrital PON fragmentation. Bacterial release, LZ excretion and unassimilated nitrogen resulting from SZ grazing are the sources of NH_4 in the model. NH_4 is converted into NO_3 through the nitrification process. Nitrogen is converted into carbon using the Redfield carbon to nitrogen (C : N) molar ratio (106 : 16; Redfield et al., 1963) and into Chl using variable C : Chl mass ratios computed according to a modified version of the phytoplankton photoacclimation model of Cloern et al. (1995).

Profiles of initial conditions were defined as the linear interpolation (1 m as in the model grid) of vertical distributions from bottle casts collected at station 345 (sampled depths are shown in Fig. 5). For NO_3 and NH_4, we used surface to 90 m deep (the maximum sampling depth at this station) concentrations averaged from 2 casts from 14 August. Below 90 m and to the end of the numerical vertical domain, we averaged concentrations ($0.02 < CV < 0.04$) from stations of the entire sampling grid for which nutrients

Full Screen / Esc

Printer-friendly Version

Interactive Discussion

were collected. For LP, we pooled together size-fractionated Chl > 20 µm (pore size 20 µm) and Chl > 5 µm (pore size 5 µm) measured on 15 August, whereas the Chl size fraction between 0.7 µm and 5 µm (pore size 0.7 µm) was used for SP. Below 90 m, null concentrations were assigned based on CTD fluorescence profiles collected on 14–15 August. Profiles of Chl concentrations were converted into nitrogen unit using the modified Cloern et al. (1985) model at time step 0 of the model run to initiate the LP and SP state variables. SZ initial concentrations in the model were obtained by subtracting the sum of vertically-interpolated biomass measurements (15 August) of phytoplankton (LP and SP, see above), detrital PON and bacteria in nitrogen unit from time coincident vertically-interpolated bottle casts measurements of PON. DONp in the model results from the vertical interpolation of DON concentrations measured on 15 August. Detrital DONl and PON were assigned a priori a constant value of $0.001\,\mathrm{mmol\,N\,m^{-3}}$ and $0.0002\,\mathrm{mmol\,N\,m^{-3}}$, respectively, at each grid point of the vertical numerical domain. Vertical boundary conditions are no flux at the sea surface (Neumann condition with vertical derivatives set to zero for all variables) and constant concentrations (Dirichlet condition) at the bottom boundary. Constant concentrations at the bottom were calculated from the linear interpolation procedure.

The set of differential equations (Table 1) was solved in a discrete form (explicit Crank-Nicolson scheme derived from the Control Volume Approach, see Roach, 1972) with Choleski's double scanning method (also called Thomas algorithm in Roach, 1972). The coupled model was run with an hourly time step. The time evolution of each of the 10 state variables (C) is computed with the general partial differential equation as follows:

$$\frac{\delta C}{\delta t} = \frac{\delta}{\delta z}\left[K_z \frac{\delta C}{\delta z}\right] + \text{source terms} - \text{loss terms}$$

where t is time, z is the vertical coordinate and K_z is the vertical eddy diffusion coefficient.

3 Results and discussion

3.1 Plankton ecosystem functioning and nitrogen fluxes

The coupled model was run in steady state mode so that the diffused state variables reached a near equilibrium state (Fig. 4) ("standard" run). Concentrations at the surface, in the DCM and integrated over the whole numerical domain tended towards near equilibrium (upper panels). This was not the case for surface NO_3 and LP. Very low NO_3 concentrations (ca. $0.003\,\mathrm{mmol\,m^{-3}}$) were quickly taken up by severely nutrient-limited LP ($\lim_N^{LP} = 0.01$). Nutrient limitation combined with increasing LZ grazing pressure on LP explained the decrease of surface LP towards concentrations near $0\,\mathrm{mmol\,N\,m^{-3}}$. As concentrations were very low, this pattern had no influence on the stability of the model. The model outputs were then compared with the time coincident multiparametric measurements (10:00 a.m. local time for all variables, except for downwelling PAR measured at 11:00 a.m. local time) (Figs. 5 and 6). The profiles of measured NO_3, NH_4, size-fractionated Chl, PON, LZ and bacterial biomass used for the comparison were same as those used to initiate the model state variables. This approach permits to assess the model ability to reproduce the observed concentrations and rates.

3.1.1 Nutrients, light, Chl and primary production

Simulated NO_3 concentrations matched their measured counterparts with concentrations being very low at the surface (ca. $0.003\,\mathrm{mmol\,N\,m^{-3}}$) and increasing with depth towards ca. $12\text{--}14\,\mathrm{mmol\,N\,m^{-3}}$ (Fig. 5a). With respect to NH_4, the measured subsurface peak (60 m) was also simulated by the model (ca. 70 m) (Fig. 5b) although the simulated concentration (ca. $0.11\,\mathrm{mmol\,N\,m^{-3}}$) was ca. 3.5-fold higher than in measurements (ca. $0.03\,\mathrm{mmol\,N\,m^{-3}}$). Note, however, that measured NH_4 exhibited much lower concentrations than generally reported in ancillary shelf seas as the Chukchi Sea ($> 1\,\mathrm{mmol\,N\,m^{-3}}$, Nishino et al., 2005). The simulated NH_4 nitrification rates within the DCM (ca. $0.0015\,\mathrm{mmol\,N\,m^{-3}\,d^{-1}}$) compared with those measured, the latter being

significant but low and likely imprecise (i.e. within the 50 % of the detection limit 0.0006–0.0008 mmol N m^{-3} d^{-1}).

With respect to phytoplankton, production rates and Chl are highly constrained by variations of the nutrients and light. The shape of the vertical light field was well reproduced by the coupled model as were the simulated PAR values at the surface and within the DCM (Fig. 6a). While the range of measured C : N ratios at study station 345 (6.744 at 3 m and 6.362 at 60 m) was analogous to the 6.625 Redfield ratio, the observed POC : Chl ratios showed a ca. 5-fold decrease from the surface (ca. 312 g g^{-1}) to the DCM (ca. 57 g g^{-1}). Assuming phytoplankton carbon can represent 20 % of POC in oligotrophic waters with a high regenerative capability (e.g. Claustre et al., 1999), the observed C : Chl range would reach ca. 62 g g^{-1} at the surface and ca. 11 g g^{-1} within the DCM. These values compare with those given by Sherr et al. (2003) and Booth and Horner (1997) for a phytoplankton assemblage dominated by < 5 µm sized cells observed in the central oligotrophic AO in summer (13–70 g g^{-1}, ca. 30 g g^{-1} on average). Furthermore, these studies report abundant picophytoplankton ecotype Micromonas as observed during the Malina cruise (Balzano et al., 2012). DuRand et al. (2002) measured Micromonas sp. cellular carbon and Chl content and estimated the mean C : Chl ratio to be ca. 30 g g^{-1}. To that respect, it can be assumed that the simulated C : Chl ratios for SP (10–45 g g^{-1}) lied within the observed range (11–63 g g^{-1}, Fig. 6b). The vertical variations of the measured light saturation parameter (E_k) (ca. 1–6 Ein m^{-2} d^{-1} within the DCM and at the surface, respectively) were reasonably captured by the model (ca. 2–16 Ein m^{-2} d^{-1} for SP within the DCM and at the surface, respectively). The C : Chl ratio and E_k are key parameters in the computation of Chl and primary production (PP) in the model.

The model produced a DCM at ca. 65 m deep with a Chl concentration of ca. 0.8 mg m^{-3} formed at 87 % by SP in agreement the observations (Fig. 5c). At the surface, the simulated SP Chl was twice (ca. 0.2 mg m^{-3}) that measured (ca. 0.1 mg m^{-3}) but values remained low. With respect to PP, the rates and shape of the profile showed comparable values and pattern in both the model and measurements (Fig. 6c). Higher

Full Screen / Esc

PP values at the surface (ca. $0.9\,\mathrm{mg\,C\,m^{-3}\,d^{-1}}$) decreased within the upper 40 m and then increased at the level of the DCM (ca. $0.6\,\mathrm{mg\,C\,m^{-3}\,d^{-1}}$ and $0.9\,\mathrm{mg\,C\,m^{-3}\,d^{-1}}$ in the observations and the model, respectively) located at ca. 65 m deep. This $0.3\,\mathrm{mg\,C\,m^{-3}\,d^{-1}}$ discrepancy at the level of the DCM was due to higher NO_3 uptake in the model (ca. $0.0025\,\mathrm{mmol\,m^{-3}\,d^{-1}}$) than in measurements (ca. $0.001\,\mathrm{mmol\,m^{-3}\,d^{-1}}$) (Fig. 6e). This also explained the higher simulated f-ratio (0.23) compared to observations (0.04).

3.1.2 Nutrients recycling

As for PP, the profiles of simulated and observed NH_4 uptake and regeneration showed similar shapes and values (Fig. 6e, f). NH_4 uptake in both measurements and the model was due to phytoplankton and bacteria. While their respective contribution is difficult to assess in-situ, phytoplankton and bacteria in the model respectively consumed 75 % and 25 % of the NH_4 pool at the surface and 60 % and 40 % within the DCM. In the data, total DCM PP (ca. $0.6\,\mathrm{mg\,C\,m^{-3}\,d^{-1}}$) would represent ca. $0.0075\,\mathrm{mmol\,N\,m^{-3}\,d^{-1}}$ using a Redfieldian ratio. Subtracting the measured regenerated PP ($0.0072\,\mathrm{mmol\,N\,m^{-3}\,d^{-1}}$) from the measured NH_4 uptake ($0.0115\,\mathrm{mmol\,N\,m^{-3}\,d^{-1}}$) would approximate the bacterial NH_4 uptake rate to $0.0043\,\mathrm{mmol\,N\,m^{-3}\,d^{-1}}$. Assuming no mixotrophy, bacteria and phytoplankton would respectively be responsible for 37 % and 63 % of the total NH_4 uptake measured at the station DCM, which was very similar to what was simulated by the coupled model.

With respect to NH_4 regeneration mostly driven in the model by SZ and bacteria, SZ and bacteria respectively contributed to 65 % and 35 % both at the surface and within the DCM. The simulated bacterial biomass was close to values measured in the upper 40 m (ca. 0.07–$0.08\,\mathrm{mg\,C\,m^{-3}}$ in average) and below the DCM (ca. 0.02–$0.03\,\mathrm{mg\,C\,m^{-3}}$ in average) but not within the DCM, where it was twice the observations (ca. $0.06\,\mathrm{mmol\,N\,m^{-3}}$ measured versus ca. $0.12\,\mathrm{mmol\,N\,m^{-3}}$ in the model) (Fig. 5e). Similarly, the simulated bacterial production matched that estimated from

measurements at the surface (ca. $0.6\,\mathrm{mgC\,m^{-3}\,d^{-1}}$) but was one order of magnitude higher in the DCM (ca. $0.9\,\mathrm{mgC\,m^{-3}\,d^{-1}}$) showing that the contribution of bacteria was likely overestimated (Fig. 6d). At this station, bacteria were found to be strictly N-limited at the surface but both N- and C-limited within the DCM (Ortega-Retuerta et al., 2012b).

5 Carbon limitation, which was not accounted in the bacterial growth model due to the large uncertainty in assessing the fraction of the measured DOC pool that can be taken up for growth, certainly explains the discrepancy. Nevertheless, the model over-estimation of bacterial biomass ($0.06\,\mathrm{mmolN\,m^{-3}}$) only had a limited impact on the DCM dynamics and simulated total PON concentration (i.e sum of phytoplankton, SZ,

10 bacteria and detrital PON) (Fig. 5d). A model run (not shown) initiated with the interpo-lated profile of measured bacterial biomass and with the steady state solutions of the "standard run" for the other 9 state variables showed that the simulated $\mathrm{NH_4}$ regener-ation (ca. $0.010\,\mathrm{mmolN\,m^{-3}\,d^{-1}}$) would still fairly approximate the measured value (ca. $0.014\,\mathrm{mmolN\,m^{-3}\,d^{-1}}$).

15 Because of its grazing activity, LZ play an important role in shaping the biomass of SZ and hence its function in nitrogen remineralization. The simulated LZ biomass showed a maximum (ca. $0.095\,\mathrm{mmolN\,m^{-3}}$) within the DCM at 60 m, as in the obser-vations (ca. $0.1\,\mathrm{mmolN\,m^{-3}}$) (Fig. 5f). In the upper 40 m, simulated values were, how-ever, one order of magnitude higher (ca. $0.05\,\mathrm{mmolN\,m^{-3}}$) than in those measured (ca.

20 $0.005\,\mathrm{mmolN\,m^{-3}}$). As no LZ diurnal migrations were set in the model, the LZ biomass varied only as a function of the biomass of prey, namely SZ at the surface. Note, how-ever, that LZ grazing (ca. $0.0012\,\mathrm{mmolN\,m^{-3}\,d^{-1}}$) was not the primary loss term of SZ biomass. It was SZ basal mortality (ca. $0.002\,\mathrm{mmolN\,m^{-3}\,d^{-1}}$) and hence the higher LZ biomass did not strongly constrain SZ in surface waters. Fecal pellets in sediment

25 traps accounted for $< 10\,\%$ ($< 1.2\,\mathrm{mgC\,m^{-2}\,d^{-1}}$) of the total flux of particulate organic matter (i.e. $12\,\mathrm{mgC\,m^{-2}\,d^{-1}}$) above (45 m) and below (90 m) the DCM (J. C. Miquel, unpublished). Using a C : N molar ratio of 8.3, the simulated PON flux was in the same range, respectively $1\,\mathrm{mgC\,m^{-2}\,d^{-1}}$ and $3.6\,\mathrm{mgC\,m^{-2}\,d^{-1}}$ at 45 m and 90 m depth.

3.2 Model sensitivity to key light-related processes

3.2.1 DON photoammonification into NH_4

In surface waters, NH_4 can be produced from the photochemical degradation of photosensitive DON mediated by the ultra-violet (UV) radiation (i.e. photoammonification; see Bushaw et al., 1996). This photochemical process was set up in the model in a simple fashion using an empirical formulation (Eq. A24 in the Appendix) linking the decrease with depth of a mean photoammonification rate within the upper 10 m (Xie et al., 2012). This approach based on measurements had been chosen at the expense of a more complex bio-optical spectral model involving accurate daily UV data, which were not available for station 345.

A simulation without the photoammonification process ("no photoammonification" run) was run in order to assess the contribution of this photochemical process to PP and its role in the plankton ecosystem functioning. During the time window simulated by the model, the the measured 10% UV irradiance depths at 325–340 nm (ca. 7.8–10.3 m), wavelengths at which most photoammonification occurred (Xie et al., 2012), were the highest encountered during the whole Malina sampling period (Para et al., 2012). A value of ca. $0.0066\,\mathrm{mmol\,m^{-2}\,d^{-1}}$ of NH_4 photo-produced from DONp was simulated by the model within the upper 10 m, which compared well with the mean value estimated from measurements in August in the same area ($0.008\,\mathrm{mmol\,N\,m^{-2}\,d^{-1}}$; Xie et al., 2012). In the model, photoammonification contributed to 13 % of the total NH_4 produced within the upper 10 m. It was the second highest source of NH_4 after the release by SZ (ca. 79 %).

A closer match with surface observations was achieved in the run accounting for the photochemical process (Figs. 7 and 8). Within the upper 10 m of the numerical domain, the simulated PON biomass was 40 % higher (53 %, 42 % and 23 % higher for bacteria, SZ and SP, respectively) than in the "no photoammonification" run (Fig. 7d). By stimulating SP and bacterial growth and subsequent SZ grazing, photoammonification contributed indirectly to 67 % of total NH_4 production and 70 % of total NH_4 uptake in

the model (Fig. 8e, f). The NH_4 photo-produced met 25 % of the simulated nitrogen demand by SP. This contribution is in line with previous estimations for the Orincco river plume (50 %; Morell and Corredor, 2001) that drains high loads of terrigenous organic matter. In terms of production, photoammonification translated into a 3.2-fold increase of the autotrophic and bacterial production (Fig. 8c, d). It is consistent with the 2.9-fold increase reported in the bioassay study of Vähätalo et al. (2011). For the whole water column, it represented a 30 % increase in the simulated PP ($37.8\,\mathrm{mg\,C\,m^{-2}\,d^{-1}}$ to $49.3\,\mathrm{mg\,C\,m^{-2}\,d^{-1}}$) and bacterial production ($37.5\,\mathrm{mg\,C\,m^{-2}\,d^{-1}}$ to $48\,\mathrm{mg\,C\,m^{-2}\,d^{-1}}$). The simulated photoammonification rate represented 6.5 % of bacterial production and was close to 2–5 % contribution given by Vähätalo et al. (2011). In the model, the photoammonification process is an important driver of the regenerative capability of the system supported by the microbial food web.

3.2.2 C : Chl ratios

In the model, the competition for resources between SP and LP was driven primarily by differences in nutrient uptake, light use and C : Chl ratios. Simulated C : Chl ratios varied according to PAR and nitrogen limitation (see Eqs. A10 and A11 in the Appendix) and constrained the light-based growth rate, which was limiting in the vicinity of DCM. LP was characterized by C : Chl ratios between 35 and $65\,\mathrm{g\,g^{-1}}$ while SP showed lower values in the 15–$45\,\mathrm{g\,g^{-1}}$ range.

Generally, biogeochemical models applied to the AO typically distinguish diatom phytoplankton from non-diatom phytoplankton. The C : Chl ratio used for diatoms generally lies between 33 and $50\,\mathrm{g\,g^{-1}}$ (Slagstad et al., 2011; Walsh et al., 2011; Zhang et al., 2011; Le Fouest et al., 2011; Popova et al., 2010), which overlaps the range simulated by the model (35 and $65\,\mathrm{g\,g^{-1}}$). However, the C : Chl ratio used for non-diatom phytoplankton varies amongst the different models. Generally invariant in space and time, it can be the same (e.g. Zhang et al., 2011; Le Fouest et al., 2010) or more than twice the value used for diatoms (83–$100\,\mathrm{g\,g^{-1}}$, e.g. Slagstad et al., 2011; Walsh et al., 2011).

These values for non-diatom phytoplankton are much higher than those simulated for SP in the model (15 and 45 g g^{-1}, Fig. 6b).

To infer the sensitivity of the model to C : Chl ratios, a simulation with a time- and depth-invariant C : Chl ratio respectively of 50 and 100 g g^{-1} for LP and SP was run ("constant C : Chl" run) and compared to the observations (Figs. 9 and 10). The simulated and measured Chl concentrations at the DCM were close (0.7–0.75 mg m^{-3}) but, contrary to the observation, LP dominated the DCM at the expense of SP (Fig. 9c). Simulated PP rates in the "standard" and "constant C : Chl" runs were comparable (0.9–0.95 mg C m^{-3} d^{-1}) but mostly new production in the "constant C : Chl" run (f-ratio of 0.63 and 0.23 in the "constant C : Chl" and "standard" runs, respectively) (Fig. 10c, e). In terms of nitrogenous biomass, LP dominated the DCM contributing to 62 % of total PON (as compared to only 18 % in the "standard" run). This increase translated into more LZ biomass (Fig. 9f) and a higher NH$_4$ concentration in the DCM resulting from more NH$_4$ release by LZ (Fig. 9b). By contrast, the activity of the microbial food web dropped within the DCM, as illustrated by the 70 % decrease of NH$_4$ regeneration (Fig. 10f) mediated by both SZ and bacteria in the model. SZ represented only 7 % of total PON in the "constant C : Chl" run, which was a much lower contribution than the 37 % simulated in the "standard" run. Similarly, the bacterial biomass and production both decreased by 50 % (Figs. 9e and 10d). C : Chl ratios involved in the simulation of the light-based phytoplankton growth rate are important drivers of the large versus small phytoplankton competition within the system.

3.3 Concluding remarks

The biological conditions encountered in the Beaufort Sea during the August 2009 Malina cruise ([Chl] = 0.7 mg m^{-3} and PP = 0.6 mg C m^{-3} d^{-1} in the DCM at the slope and ice-edge study station 345) strikingly contrasted with those reported in summer in similar environments in the Chukchi, Barents and Western Beaufort seas ((Chl) = 2–11 mg m^{-3} and PP = 10–300 mg C m^{-3} d^{-1}; Zhang et al., 2011; Matrai et al., 2007; Reigstad et al., 2002). In this context, a 1-D physical-biological coupled model was

Title Page

Abstract | Introduction

Conclusions | References

Tables | Figures

◄ | ►|

◄ | ►

Back | Close

Full Screen / Esc

Printer-friendly Version

Interactive Discussion

developed to gain a better understanding of the plankton ecosystem functioning in these stratified, clear and very oligotrophic offshore waters. The coupled model was forced by a stationary field of vertical turbulent diffusion and by a diurnal cycle of surface PAR based on measurements at station 345. Simulations at steady state were produced and the outputs compared to an extensive dataset of space and time coincident and multiparametric data sampled at the same station.

The 10-compartment ecosystem model approximated the observed nitrogen fluxes and biomass levels. It suggested that NH_4 photo-produced from DONp was a necessary nitrogen source to achieve the observed levels of autotrophic and heterotrophic biomass and production. The photo-chemical process fueled SP regenerated PP directly through the NH_4 uptake by SP and indirectly by stimulating the heterotrophic protists activity. Increased SP growth stimulated grazing and the subsequent release of NH_4 and DONl by SZ. NH_4 was used up by both SP and bacteria while the latter also beneficiated from DONl for growth. Increased bacterial growth led to an increased bacterial release of NH_4. Photoammonification occurring within the upper 10 m of the water column contributed to ca. one-third of the simulated depth-integrated primary and bacterial daily production rates. The model also suggested that C : Chl ratios (83–100 $g g^{-1}$) typically used for the non-diatom phytoplankton compartment in plankton ecosystem models applied to the AO were not appropriate to reproduce the plankton ecosystem structure of the oligotrophic Beaufort Sea. Applying such ratios in the model led to a DCM dominated by large phytoplankton ensuring mostly new PP, whereas observations reported an autotrophic community dominated by small phytoplankton growing essentially on regenerated nitrogen. Relatively low C : Chl ratios (ca. 15–45 $g g^{-1}$) for small phytoplankton were required to simulate the observed herbivorous versus microbial food web competition and realistic nitrogen fluxes within the DCM.

The accelerated sea ice shrinking and thinning might promote in the AO deep changes in autotrophic and heterotrophic biomass levels, production rates and carbon export (Wassmann and Reigstad, 2011; Boyce et al., 2010; Li et al., 2009, Arrigo et al., 2008). Enhanced stratification and nutrient limitation already suggest the increasing

Printer-friendly Version

Interactive Discussion

role of the microbial food web in the plankton ecosystem (Li et al., 2009; Tremblay et al., 2009). In this context and in view of the current modeling effort in assessing the oceanic (e.g. Le Fouest et al., 2010; Popova et al., 2010) and continental (e.g. Tank et al., 2011) drivers for AO primary production, more attention should be paid in the future to the mechanistic processes involved in food webs and functional groups competition, nutrient recycling and primary production in poorly productive Arctic waters as they are expected to expand rapidly (Wassmann and Reigstad, 2011). In particular, the still debated real contribution of the summer DCM in the annual primary production budget should be clarified (e.g. Ardyna et al., 2012; Popova et al., 2010). Such a better knowledge is required for robust model projections of AO primary production and carbon fluxes in response to the accelerated warming.

Appendix A

The set of differential equations that include the mechanistic formulations cited below is given in Table 1. The biological parameters related to the mathematical equations are detailed in Table 2.

A1 Phytoplankton

The growth rate ($\mu^{\mathrm{LP,SP}}$, d^{-1}) of large and small phytoplankton (LP and SP, respectively) depends on both light and nitrogen availability. It is computed according to the Liebig's Law of the minimum between the nutrient-based and light-based growth rates ($\mu_{\mathrm{N}}^{\mathrm{LP,SP}}$ and $\mu_{\mathrm{light}}^{\mathrm{LP,SP}}$, respectively):

$$\mu^{\mathrm{LP,SP}} = \min\left(\mu_{\mathrm{N}}^{\mathrm{LP,SP}}, \mu_{\mathrm{light}}^{\mathrm{LP,SP}}\right) \tag{A1}$$

Arctic plankton modeling

V. Le Fouest et al.

The nutrient-based growth rate is computed as follows:

$$\mu_N^{LP,SP} = \mu_{max}^{LP,SP} \lim_N^{LP,SP} \tag{A2}$$

where $\mu_{max}^{LP,SP}$ is the maximum growth rate and $\lim_N^{LP,SP}$ the total nutrient limitation term (dimensionless) computed according to the substitutable model of O'Neill et al. (1989):

$$\lim_N^{LP,SP} = \frac{NO_3 K_{NH_4}^{LP,SP} + NH_4 K_{NO_3}^{LP,SP}}{NO_3 K_{NH_4}^{LP,SP} + NH_4 K_{NO_3}^{LP,SP} + K_{NH_4}^{LP,SP} K_{NO_3}^{LP,SP}} \tag{A3}$$

$$\lim_{NO_3}^{LP,SP} = \frac{NO_3 K_{NH_4}^{LP,SP}}{NO_3 K_{NH_4}^{LP,SP} + NH_4 K_{NO_3}^{LP,SP}} \tag{A4}$$

$$\lim_{NH_4}^{LP,SP} = \frac{NH_4 K_{NO_3}^{LP,SP}}{NO_3 K_{NH_4}^{LP,SP} + NH_4 K_{NO_3}^{LP,SP}} \tag{A5}$$

where $\lim_{NO_3}^{LP,SP}$ and $\lim_{NH_4}^{LP,SP}$ are the nitrate (NO_3) and ammonium (NH_4) uptake fractions, respectively. $K_{NH_4}^{LP,SP}$ and $K_{NO_3}^{LP,SP}$ are the half-saturation constants for NH_4 and NO_3 uptake, respectively. NH_4 is set to be the preferred inorganic nitrogen source (Dorch, 1990) with a higher affinity for SP (Tremblay et al., 2000). This is expressed in the model by half-saturation constants for NH_4 uptake ($K_{NH_4}^{LP,SP}$) significantly lower than for NO_3 that, when used with the substitutable model, allow for an inhibitory effect of NH_4 on NO_3 uptake as often observed (Dorch, 1990). The equation used to compute the light-based growth rate is:

$$\mu_{light}^{LP,SP} = \mu_{max}^{LP,SP} \lim_{light}^{LP,SP} \tag{A6}$$

Arctic plankton modeling

V. Le Fouest et al.

Title Page

Abstract	Introduction
Conclusions	References
Tables	Figures

Back | Close

Full Screen / Esc

Printer-friendly Version

Interactive Discussion

where $\lim_{\text{light}}^{\text{LP,SP}}$ is the light limitation term (dimensionless) expressed as:

$$\lim_{\text{light}}^{\text{LP,SP}} = 1 - e^{-\frac{E_z}{E_k^{\text{LP,SP}}}} \tag{A7}$$

where $E_k^{\text{LP,SP}}$ is the light saturation parameter ($\text{Ein}\,\text{m}^{-2}\,\text{d}^{-1}$) computed as follows:

$$E_k^{\text{LP,SP}} = \left(\frac{\text{C}}{\text{Chl}}\right)^{\text{LP,SP}} \frac{\mu_{\max}^{\text{LP,SP}}}{\alpha_{\text{LP,SP}}} \tag{A8}$$

5 where $\frac{\text{C}}{\text{Chl}}$ is the carbon to Chl ratio ($\text{g}\,\text{g}^{-1}$) and $\alpha_{\text{LP,SP}}$ the initial slope ($\text{mg}\,\text{C}\,(\text{mg}\,\text{Chl})^{-1}\,(\text{Ein}\,\text{m}^{-2}\,\text{d}^{-1})^{-1}$) of the photosynthesis-irradiance curve. Photoacclimation translates the adaptative response through varying Chl : C ratios in response to light and nutrient availability (e.g. Cloern et al., 1995; Geider et al., 1997; MacIntyre et al., 2002). Values of $\alpha_{\text{LP,SP}}$ were measured during the Malina cruise

10 at 0–3 m and 65 m deep. In average for the study station 345, values of $\alpha_{\text{LP,SP}}$ showed a decrease from the surface ($2.22\,\text{mg}\,\text{C}\,(\text{mg}\,\text{Chl})^{-1}\,(\text{Ein}\,\text{m}^{-2}\,\text{d}^{-1})^{-1}$) to the DCM ($6.94\,\text{mg}\,\text{C}\,(\text{mg}\,\text{Chl})^{-1}\,(\text{Ein}\,\text{m}^{-2}\,\text{d}^{-1})^{-1}$). A linear function relating $\alpha_{\text{LP,SP}}$ to depth is set from the surface to 65 m to account for this decrease:

$$\alpha_{\text{LP,SP}} = 0.0826315z + 1.9721055 \tag{A9}$$

15 A constant value of $5.55\,\text{mg}\,\text{C}\,(\text{mg}\,\text{Chl})^{-1}\,(\text{Ein}\,\text{m}^{-2}\,\text{d}^{-1})^{-1}$ is set below 65 m based on reported measurements.

Varying Chl : C ratios are computed using a modified version of the empirical relationship of Cloern et al. (1995) successfully applied to Hudson Bay in the Arctic (Sibert et al., 2011). The ratios can vary up to 4- to 6-fold based on the general photoacclima-

20 tion rule given by MacIntyre et al. (2002) and on Arctic nano- and picophytoplankton

data (DuRand et al., 2002; Sherr et al., 2003) as follows:

$$\left(\frac{\text{Chl}}{\text{C}}\right)^{\text{LP}} = \left(\frac{\text{Chl}}{\text{C}}\right)_{\text{max LP}} \left(1 + 4e^{-0.50\frac{E_z}{\kappa_E^{\text{LP}}}\lim_N^{\text{LP}}}\right) \tag{A10}$$

$$\left(\frac{\text{Chl}}{\text{C}}\right)^{\text{SP}} = \left(\frac{\text{Chl}}{\text{C}}\right)_{\text{max SP}} \left(1 + 6e^{-0.5\frac{E_z}{\kappa_E^{\text{SP}}}\lim_N^{\text{SP}}}\right) \tag{A11}$$

where $K_E^{\text{LP,SP}}$ is the half saturation parameter driving the curvature of the Chl : C versus light relationship. E_z (Ein m^{-2} d^{-1}) is the downwelling PAR propagating according to the Beer-Lambert's law:

$$E_z = \text{PAR0} \int e^{-[(\text{kchl}+\text{kw}+\text{knonchl})z]} dz \tag{A12}$$

where the diffuse attenuation of PAR with depth (z) is due to the simulated Chl (kchl) (m^{-1}; Morel, 1988), water molecules (kw) (0.04 m^{-1}; Morel, 1988) and non-chlorophyllous matter (knonchl). knonchl is set to 0.05 m^{-1} from 0 to 5 m depth to account for the release of optically active matter by melting sea ice observed during Malina (Doxaran et al., 2012) and to 0 below. kchl is calculated according to Morel et al. (1988) as follows:

$$\text{kchl} = 0.0518\text{Chl}^{-0.572}\text{Chl} \tag{A13}$$

with

$$\text{Chl} = 12\left(\frac{106}{16}\right)\left[\left(\frac{\text{Chl}}{\text{C}}\right)^{\text{LP}}\text{LP} + \left(\frac{\text{Chl}}{\text{C}}\right)^{\text{SP}}\text{SP}\right] \tag{A14}$$

Apart from grazing, phytoplankton loss terms include basal mortality and sinking for LP. LP sinking rates vary in the model from 0 to 0.1 m d^{-1} (e.g. Smith et al., 1991) depending on nutrients availability (Bienfang et al., 1983):

$$\text{sedlp} = \text{sed\_lp}\left(1 - \lim_N^{\text{LP}}\right) \tag{A15}$$

A2 Zooplankton

Mathematical formulations and parameters related to large zooplankton (LZ) dynamics were chosen to reflect copepods as they dominate in abundance at the study station (Forest et al., 2012). Grazing (d^{-1}) is described by an Ivlev function:

$$G_{LZ} = G_{LZ}^{max} \left[\left(1 - e^{-\lambda(LP+SZ)} \right) \right] \tag{A16}$$

LZ graze upon LP and protozooplankton (SZ) with a prey-specific grazing rate assumed to be proportional to the relative biomass of the prey (Campbell et al., 2009) defined for LP as follows:

$$pf_{LP} = \frac{LP}{LP + SZ} \tag{A17}$$

Losses in LZ biomass are due to NH_4 release, fecal pellets production (non-assimilated nitrogen ingested) and mortality. Mortality is assumed to be mainly due to predation (Eiane et al., 2002) and is described by a density-dependant quadratic function. The latter implicitly represents cannibalism as well as predation by appendicularians observed during the Malina cruise (Forest et al., 2012) and limits the occurrence of oscillations generated in such non-linear systems (Edwards and Bees, 2001). The constant of mortality is set to $0.2 \, (\text{mmol} \, N \, m^{-3})^{-1}$ to simulate realistic mortality rates (e.g. Ohman et al., 2004).

SZ grazing upon SP and bacteria (BACT) is formulated by a sigmoid "Holling-type-III" function:

$$G_{SZ} = G_{SZ}^{max} \frac{(SP + BACT)^2}{(SP + BACT)^2 + K_G^2} \tag{A18}$$

The function provides a threshold-like limit for low SP biomass that enhances the biological system stability (e.g. Steele and Henderson, 1992). In polar waters, there is

Full Screen / Esc

Printer-friendly Version

Interactive Discussion

evidence that protozooplankton exert a control on small phytoplankton biomass only beyond a threshold (Lancelot et al., 1997). As for LZ, SZ graze upon both SP and BACT with a prey-specific grazing rate (d^{-1}) assumed to be proportional to the relative biomass of the prey defined for SP as follows:

$$pf_{SP} = \frac{SP}{SP + BACT} \tag{A19}$$

According to the study of Riegman et al. (1993), we set the fraction of food ingested by SZ and being converted into biomass to 30 %. Lehrter et al. (1999) report that > 30 % of the total nitrogen release by SZ could be in the dissolved organic form. In the model, assuming that 40 % is released as labile DON (DONl), the remaining 30 % are lost as NH_4. Remaining SZ loss terms are grazing by LZ and mortality. Similarly to LZ, mortality is expressed by a density-dependant quadratic function to represent grazing amongst SZ.

A3   Bacteria

Bacteria are explicitly simulated following the model of Fasham et al. (1990). DONl is the preferred substrate for bacterial uptake (d^{-1}) (Kirchman et al., 1989) represented by a Michaelis-Menten model:

$$Ubact_{DONl} = Ubact_{max}BACT\left(\frac{DONl}{K_{NH_4,DONl}^{BACT} + S + DONl}\right) \tag{A20}$$

where $Ubact_{max}$ is the maximum uptake rate, $K_{NH_4,DONl}^{BACT}$ ($mmol\,N\,m^{-3}$) the half-saturation constant for uptake and S the total nitrogenous substrate ($mmol\,N\,m^{-3}$) defined as:

$$S = (NH_4, 0.6DONl) \tag{A21}$$

Similarly, the uptake of NH_4 is represented as follows:

$$\text{Ubact}_{NH_4} = \text{Ubact}_{max}\text{BACT}\left(\frac{S}{K_{NH_4,DONI}^{BACT} + S + DONI}\right) \tag{A22}$$

This formulation ensures that the uptake of NH_4 will be 0.6 times the uptake of DONI, as required by the balanced growth model (e.g. Fasham et al., 1990). Bacterial losses are in the NH_4 form and represent 5 % of the bacterial biomass.

A4 Detritus

The pool of detrital particulate organic nitrogen (PON) is fueled by LZ fecal pellets production and by LZ and LP mortality. The sedimentation loss term (d^{-1}) is expressed as a quadratic function allowing for increasing implicit aggregation of particles with increasing PON concentrations:

$$\text{sedpon} = \text{sed\_ponPON} \tag{A23}$$

where sed_pon is the sedimentation constant ($m\,d^{-1}\,(mmol\,N\,m^{-3})^{-1}$). The second loss term is the bacteria-mediated PON fragmentation into DONI (Grossart and Ploug, 2001).

The DONI pool results from detrital PON fragmentation, SP and SZ mortality and SZ release. It is explicitly remineralized into NH_4 by bacteria. Based on measurements made in the Beaufort Sea in summer and during the Malina cruise (Xie et al., 2012), we incorporated the photochemical production of NH_4 from DONp (i.e. photoammonification) ($mmol\,N\,m^{-3}\,d^{-1}$) within the first 10 m of the water column:

$$\text{ammo} = 10\frac{0.00004}{z}\text{DONp} \tag{A24}$$

The mean constant rate for the June–August period was estimated to ca. $0.00016\,d^{-1}$. For mid-August, when the model is run, a value of $0.00004\,d^{-1}$ is chosen to produce

Full Screen / Esc

Printer-friendly Version

Interactive Discussion

NH$_4$ photo-production rates comparable to those measured in late summer. Below 10 m, the rate is set to 0.

A5 Nutrients

NH$_4$ resulting from bacterial remineralization, photoammonification of DONp as well as the release by LZ and SZ fuels the regenerated primary production and bacterial production. In turn, NH$_4$ is undergoes nitrification (d^{-1}) into NO$_3$ as follows:

$$
\text{nitrif} = \text{nitrif}_{max} \left(\frac{NH_4}{NH_4 + K^N_{nitrif}} \right) \left(1 - \frac{E_z}{E_z + K^{light}_{nitrif}} \right)
\tag{A25}
$$

Where nitrif$_{max}$ is the maximum nitrification rate and K^N_{nitrif} and K^{light}_{nitrif} the half-saturation constants for NH$_4$ (mmol N m^{-3}) and light (E in m^{-2} d^{-1}) use, respectively. The latter is defined as a fraction of surface PAR (E_0) as follows:

$$
K^{light}_{nitrif} = 0.005 E_0
\tag{A26}
$$

Back | Close

Full Screen / Esc

Printer-friendly Version

Interactive Discussion

References

Ardyna, M., Gosselin, M., Michel, C., Poulin, M., and Tremblay, J.-E.: Environmental forcing of phytoplankton community structure and function in the Canadian High Arctic: contrasting oligotrophic and eutrophic regions, Mar. Ecol. Prog. Ser., 442, 37–57, 2011.

Ardyna, M., Babin, M., Gosselin, M., Devred, E., Bélanger, S., Matsuoka, A., and Tremblay, J.-E.: Parameterization of the vertical chlorophyll-a in the Arctic Ocean: impact of subsurface chlorophyll maximum to regional, seasonal and annual primary production estimates, Biogeosciences Discuss., submitted, 2012.

Arrigo, K. R. and van Djiken, G. L.: Secular trends in Arctic Ocean net primary production, J. Geophys. Res., 116, C09011, doi:10.1029/2011JC007151, 2011.

Arrigo, K. R., van Dijken, G., and Pabi, S.: Impact of a shrinking Arctic ice cover on marine primary production, Geophys. Res. Lett., 35, L19603, doi:10.1029/2008GL035028, 2008.

Balzano, S., Marie, D., Gourvil, P., and Vaulot, D.: Composition of the summer photosynthetic pico and nanoplankton communities in the Beaufort Sea assessed by T-RFLP and sequences of the 18S rRNA gene from flow cytometry sorted samples, ISME J., 6, 1480–1498, doi:10.1038/ismej.2011.213, 2012.

Bélanger, S., Babin, M., and Tremblay, J.-E.: Increasing cloudiness in Arctic damps the increase in phytoplankton primary production due to sea ice receding, Biogeosciences Discuss., 9, 13987–14012, doi:10.5194/bgd-9-13987-2012, 2012.

Bienfang, P., Szyper, J., and Laws, E.: Sinking rate and pigment responses to light limitation of a marine diatom: implications to dynamics of chlorophyll maximum layers, Oceanologica Acta 6, 55–62, 1983.

Booth, B. C. and Horner, R. A.: Microalgae on the Arctic Ocean Section, 1994: species abundance and biomass, Deep-Sea Res. Pt. II, 44, 1607–1622, 1997.

Boyce, D. G., Lewis, M. R., and Worm, B.: Global phytoplankton decline over the past century, Nature, 466, 591–596, doi:10.1038/nature09268, 2010.

5 Bushaw, K. L., Zepp, R. G., Tarr, M. A., Schultz-Jander, D., Bourbonniere, R. A., Hodson, R. E., Miller, W. L., Bronk, D. A., and Moran, M. A.: Photochemical release of biologically available nitrogen from aquatic dissolved organic matter, Nature, 381, 404–407, 1996.

Campbell, R. G., Sherr, E. B., Ashjian, C. J., Plourde. S., Sherr, B. F., Hill, V., and Stockwell, D. A.: Mesozooplankton prey preference and grazing impact in the Western Arctic

10 Ocean, Deep-Sea Res. Pt. II, 56, 1274–1289, doi:10.1016/j.dsr2.2008.10.027, 2009.

Claustre, H., Morel, A., Babin, M., Cailliau, C., Marie, D., Marty, J.-C., and Vaulot, D.: Variability in particle attenuation and stimulated fluorescence in the Tropical and Equatorial Pacific: scales, patterns and some biogeochemical implications, J. Geophys. Res., 104, 3401–3422, 1999.

15 Cloern, J. E., Grenz, C., and Videgar-Lucas, L.: An empirical model of the phytoplankton chlorophyll : carbon ratio – the conversion factor between productivity and growth rate, Limnol. Oceanogr., 40, 1313–1321, 1995.

Dorch, Q.: The interaction between ammonium and nitrate uptake in phytoplankton, Mar. Ecol. Prog. Ser., 61, 183–201, 1990.

20 Doxaran, D., Ehn, J., Bélanger, S., Matsuoka, A., Hooker, S., and Babin, M.: Optical characterisation of suspended particles in the Mackenzie River plume (Canadian Arctic Ocean) and implications for ocean colour remote sensing, Biogeosciences, 9, 3213–3229, doi:10.5194/bg-9-3213-2012, 2012.

DuRand, M. D., Green, R. E., Sosik, H. M., and Olson, R. J.: Diel variations in optical properties

25 of *Micromonas pusilla* (Prasinophyceae), J. Phycol., 38, 1132–1142, 2002.

Edwards, A. M. and Bees, M. A.: Generic dynamics of a simple plankton population model with a non-integer exponent of closure, Chaos Soliton. Fract., 12, 289–300, 2001.

Eiane, K., Aksnes, D. L., Ohman, M. D., Wood, S., and Martinussen, M. B.: Stage-specific mortality of *Calanus* spp. under different predation regimes, Limnol. Oceanogr., 47, 636–

30 645, 2002.

Fasham, M. J. R., Ducklow, H. W., and McKelvie, S. M.: A nitrogen-based model of plankton dynamics in the oceanic mixed layer, J. Mar. Res., 48, 591–639, 1990.

Arctic plankton modeling

V. Le Fouest et al.

Forest, A., Galindo, V., Darnis, G., Pineault, S., Lalande, C., Tremblay, J.-E., and Fortier, L.: Carbon biomass, elemental ratios (C : N) and stable isotopic composition (δ^{13}C, δ^{15}N) of dominant calanoid copepods during the winter-to-summer transition in the Amundsen Gulf (Arctic Ocean), J. Plankton. Res., 33, 161–178, 2010.

Forest, A., Stemmann, L., Picheral, M., Burdorf, L., Robert, D., Fortier, L., and Babin, M.: Size distribution of particles and zooplankton across the shelf-basin system in southeast Beaufort Sea: combined results from an Underwater Vision Profiler and vertical net tows, Biogeosciences, 9, 1301–1320, doi:10.5194/bg-9-1301-2012, 2012.

Geider, R. J., MacIntyre, H. L., and Kana, T. M.: Dynamic model of phytoplankton growth and acclimation: responses of the balanced growth rate and the chlorophyll-*a*: carbon ratio to light, nutrient-limitation and temperature, Mar. Ecol. Prog. Ser., 148, 187–200, 1997.

Grossart, H.-P. and Ploug, H.: Microbial degradation of organic carbon and nitrogen on diatom aggregates, Limnol. Oceanogr., 46, 267–277, 2001.

Holmes, M. R., Aminot, A., Kerouel, R., Hooker, B. A., and Peterson, J. B.: A simple and precise method for measuring ammonium in marine and freshwater ecosystems, Can. J. Fish Aquat. Sci., 56, 1801–1808, 1999.

Hooker, S. B., Morrow, J. H., and Matsuoka, A.: The 1 % and 1 cm perspective in deriving and validating AOP data products, Biogeosciences Discuss., 9, 9487–9531, doi:10.5194/bgd-9-9487-2012, 2012.

Huot Y., Babin, M., and Bruyant, F.: Photosynthetic parameters in the Beaufort Sea in relation with the phytoplankton community structure, Biogeosciences Discuss., submitted, 2012.

Kahru, M., Brotas, V., Manzano-Sarabia, M., and Mitchell, B. G.: Are phytoplankton blooms occurring earlier in the Arctic?, Global Change Biol., 17, 1733–1739, doi:10.1111/j.1365-2486.2010.02312.x, 2011.

Kichman, D. L., Kiel, R. G., and Wheeler, P. A.: The effect of amino acids on ammonium utilization and regeneration by heterotrophic bacteria in the Subarctic Pacific, Deep-Sea Res., 36, 1763–1776, 1989.

Kirchman, D. L., Hill, V., Cottrell, M. T., Gradinger, R., Malmstrom, R. R., and Parker, A.: Standing stocks, production, and respiration of phytoplankton and heterotrophic bacteria in the Western Arctic Ocean, Deep-Sea Res. Pt. II, 56, 1237–1248, doi:10.1016/j.dsr2.2008.10.018, 2009.

Title Page

Abstract | Introduction

Conclusions | References

Tables | Figures

|◀ | ▶|

◀ | ▶

Back | Close

Full Screen / Esc

Printer-friendly Version

Interactive Discussion

Le Fouest, V., Postlethwaite, C., Morales Maqueda, M. A., Bélanger, S., and Babin, M.: On the role of tides and strong wind events in promoting summer primary production in the Barents Sea, Cont. Shelf Res., 31, 1869–1879, doi:10.1016/j.csr.2011.08.013, 2011.

Lancelot, C., Becquevort, S., Menon, P., Mathot, S., and Dandois, J.-M.: Ecological modelling of the planktonic microbial food-web, in: Belgian Research Program on the Antarctic, Scientific Results of Phase III (1992–1996): Marine Biogeochemistry and Ecodynamics, vol. 1, edited by: Caschetto, S., Fed. Off. for Sci., Tech. and Cult. Affairs, Brussels, 1–78, 1997.

Lehrter, J. C., Pennock, J. R., and McManus, G. B.: Microzooplankton grazing and nitrogen excretion across a surface estuarine-coastal interface, Estuaries, 22, 113–125, 1999.

Li, W. K. W., McLaughlin, F. A., Lovejoy, C., and Carmack, E. C.: Smallest algae thrive as the Arctic Ocean freshens, Science, 326, 539, doi:10.1126/science.1179798, 2009.

MacIntyre, H. L., Kana, T. M., Anning, T., and Geider, R. J.: Photoacclimation of photosynthesis irradiance response curves and photosynthetic pigments in microalgae and cyanobacteria, J. Phycol., 38, 17–38, 2002.

Martin, J., Tremblay, J. E., Gagnon, J., Tremblay, G., Lapoussière, A., Jose, C., Poulin, M., Gosselin, M., Gratton, Y., and Michel, C.: Prevalence, structure and properties of sub-surface chlorophyll maxima in Canadian Arctic waters, Mar. Ecol. Prog. Ser., 42, 69–84, doi:10.3354/meps08666, 2010.

Matrai, P., Vernet, M., and Wassmann, P.: Relating temporal and spatial patterns of DMSP in the Barents Sea to phytoplankton biomass and productivity, J. Marine Syst., 67, 83–101, doi:10.1016/j.jmarsys.2006.10.001, 2007.

Morel, A.: Optical modeling of the upper ocean in relation to its biogenous matter content (case I waters), J. Geophys. Res., 93, 10749–10768, 1988.

Morell, J. and Corredor, J.: Photomineralization of fluorescent dissolved organic matter in the Orinoco River plume: estimation of ammonium release, J. Geophys. Res., 106, 16807–16813, doi:10.1029/1999JC000268, 2001.

Nishino, S., Shimada, K., and Motoyo, I.: Use of ammonium and other nitrogen tracers to investigate the spreading of shelf waters in the Western Arctic halocline, J. Geophys. Res., 110, C10005, doi:10.1029/2003JC002118, 2005.

O'Neill, R. V., DeAngelis, D. L., Pastor, J. J., Jackson, B. J., and Post, W. M.: Multiple nutrient limitations in ecological models, Ecol. Model., 46, 147–163, 1989.

Title Page

Abstract | Introduction

Conclusions | References

Tables | Figures

◄ | ►

◄ | ►

Back | Close

Full Screen / Esc

Printer-friendly Version

Interactive Discussion

Ohman, M. D., Eiane, K., Durbin, E. G., Runge, J. A., and Hirche, H.-J.: A comparative study of Calanus finmarchicus mortality patterns at five localities in the North Atlantic, ICES J. Mar. Sci., 61, 687–697, 2004.

Ortega-Retuerta, E., Jeffrey, W. H., Babin, M., Bélanger, S., Benner, R., Marie, D., Matsuoka, A., Raimbault, P., and Joux, F.: Carbon fluxes in the Canadian Arctic: patterns and drivers of bacterial abundance, production and respiration on the Beaufort Sea margin, Biogeosciences, 9, 3679–3692, doi:10.5194/bg-9-3679-2012, 2012a.

Ortega-Retuerta, E., Jeffrey, W. H., Ghiglione, J.-F., and Joux, F.: Evidence of heterotrophic prokaryotic activity limitation by nitrogen in the Western Arctic Ocean during summer, Polar Biol., 35, 785–794, 2012b.

Osborn, T. R.: Estimates of the local rate of vertical diffusion from dissipation measurements, J. Phys. Oceanogr., 10, 83–89, 1980.

Para, J., Charrière, B., Matsuoka, A., Miller, W. L., Rontani, J. F. R., and Sempéré, R.: UV radiation and DOM properties in surface coastal waters of the Canadian shelf of the Beaufort Sea during summer 2009, Biogeosciences Discuss., submitted, 2012.

Popova, E. E., Yool, A., Coward, A. C., Aksenov, Y. K., Alderson, S. G., de Cuevas, B. A., and Anderson, T. R.: Control of primary production in the Arctic by nutrients and light: insights from a high resolution ocean general circulation model, Biogeosciences, 7, 3569–3591, doi:10.5194/bg-7-3569-2010, 2010.

Raimbault, P., Slawyk, G., Coste, B, and Fry, J.: Feasibility of using an automated colorimetric procedure for the determination of seawater nitrate in the 0 to 100 nM range: examples from field and culture, Mar. Biol., 104, 347–351, 1990.

Raimbault, P., Slawyk, G., Boudjellal, B., Coatanoan, C., Conan, P., Coste, B., Garcia, N., Moutin, T., and Pujo-Pay, M.: Carbon and nitrogen uptake and export in the equatorial pacific at 150° W: evidence of an efficient regenerated production cycle, J. Geophys. Res., 104, 3341–3356, 1999.

Redfield, A. C., Ketchum, B. H., and Richards, F. A.: The influence of organisms on the composition of sea water, in: The Sea: Ideas and Observations on Progress in the Study of the Seas, edited by: M. N. Hill, Wiley-Intersci., Hoboken, NY, 26–27, 1973.

Reigstad, M., Wassmann, P., Wexels Riser, C., Øygarden, S., and Rey, F.: Variations in hydrography, nutrients and chlorophyll-*a* in the marginal ice-zone and the Central Barents Sea, J. Marine Syst., 38, 9–29, doi:10.1016/S0924-7963(02)00167-7, 2002.

Riegman, R., Kuipers, B. R., Nooedeloos, A. A. M., and Witte, H. J.: Size-differential control of phytoplankton and the structure of plankton communities, Neth. J. Sea Res., 31, 255–265, 1993.

Roach, P. J.: Computational Fluid Dynamics, Hermosa, Albuquerque, NM, 446 pp., 1972.

5   Sakshaug, E.: Primary and secondary production in the Arctic seas, in: The Organic Carbon Cycle in the Arctic Ocean, edited by: Stein, R. and MacDonald, R. W., Springer-Verlag, Berlin, 57–81, 2004.

Sherr, E. B., Sherr, F. B., Wheeler, P. A., and Thompson, K.: Temporal and spatial variation in stocks of autotrophic and heterotrophic microbes in the upper water column of the Central Arctic Ocean, Deep-Sea Res. Pt. I, 50, 557–571, doi:10.1016/S0967-0637(03)00031-1, 2003.

Sibert, V., Zakardjian, B., Gosselin, M., Starr, M., Senneville, S., and LeClainche, Y.: 3-D biophysical model of the sympagic and planktonic productions in the Hudson Bay System, J. Marine Syst., 88, 401–422, doi:10.1016/j.jmarsys.2011.03.014, 2011.

15 Slagstad, D., Ellingsen, I. H., and Wassmann, P.: Evaluating primary and secondary production in an Arctic Ocean void of summer sea ice: an experimental simulation approach, Prog. Oceanogr., 90, 117–131. doi:10.1016/j.pocean.2011.02.009, 2011.

Smith Jr., W. O., Kelly, H. P., and Vogelin, D.: Phytoplankton Sinking Rates in the Ross Sea, Antarctic Journal of the United States, 151–152, 1991.

20 Steele, J. H. and Henderson, E. W.: The role of predation in plankton models, J. Plankton Res., 14, 157–172, 1992.

Tank, S. E., Manizza, M., Holmes, R. M., McClelland, J. W., and Peterson, B. J.: The processing and impact of dissolved riverine nitrogen in the Arctic Ocean, Estuar. Coast., 35, 401–415, doi:10.1007/s12237-011-9417-3, 2011.

25 Tremblay, J.-E. and Gagnon, J.: The effects of irradiance and nutrient supply on the productivity of Arctic waters: a perspective on climate change, in: Influence of Climate Change on the Changing Arctic and Subarctic Conditions, edited by: Nihoul, J. C. J. and Kostianoy, A. G., NATO Science for Peace and Security Series-C: Environmental Security, Springer Science, Berlin, 73–93, 2009.

30 Tremblay, J.-E., Legendre, L., Klein, B., and Therriault, J.-C.: Size differential uptake of nitrogen and carbon in a marginal sea (Gulf of St. Lawrence, Canada): significance of diel periodicity and urea uptake, Deep Sea Res. Pt. II, 47, 489–518, 2000.

Tremblay, J.-E., Simpson, K., Martin, J., Miller, L., Gtatton, Y., Barber, D., and Price, N. M.: Vertical stability and the annual dynamics of nutrients and chlorophyll fluorescence in the coastal, Southeast Beaufort Sea, J. Geophys. Res.-Oceans, 113, C07S90, doi:10.1029/2007JC004547, 2008.

5 Tremblay, J.-E., Raimbault, P., Garcia, N., and Gagnon, J.: Distribution of nutrients and organic carbon, nitrogen and phosphorus in the Southeast Beaufort Sea: implications for primary, Biogeosciences Discuss., submitted, 2012.

Vähätalo, A. V., Aarnos, H., Hoikkala, L., and Lignell, R.: Photochemical transformation of ter-restrial dissolved organic matter supports hetero- and autotrophic production in coastal wa-

10 ters, Mar. Ecol. Prog. Ser., 423, 1–14, doi:10.3354/meps09010, 2011.

Walsh, J. J., Dieterle, D. A., Chen, R., Lenes, J. M., Maslowski, W., Cassano, J. J., Whitledge, T. E., Stockwell, D., Flint, M., Sukhanova, I. N., and Christensen, J.: Trophic cas-cades and future harmful algal blooms within ice-free Arctic Seas north of Bering Strait: a simulation analysis, Prog. Oceanogr., 91, 312–343, doi:10.1016/j.pocean.2011.02.001,

15 2011.

Wassmann, P. and Reigstad, M.: Future Arctic Ocean seasonal ice zones and implications for pelagic-benthic coupling, Oceanography, 24, 220–231, doi:10.5670/oceanog.2011.74, 2011.

Wheeler, P. A., Watkins, J. M., and Hansing, R. L.: Nutrients, organic carbon and organic nitro-

20 gen in the upper water column of the Arctic Ocean: implications for the sources of dissolved organic carbon, Deep-Sea Res. Pt. II, 44, 1571–1592, 1997.

Xie, H., Bélanger, S., Song, G., Benner, R., Taalba, A., Blais, M., Tremblay, J.-É., and Babin, M.: Photoproduction of ammonium in the southeastern Beaufort Sea and its biogeochemical implications, Biogeosciences, 9, 3047–3061, doi:10.5194/bg-9-3047-2012, 2012.

25 Zhang, J., Spitz, Y. H., Steele, M., Ashjian, C., Campbell, R., Berline, L., and Matrai, P.: Modeling the impact of declining se ice on the Arctic marine planktonic ecosystem. J. Geophys. Res., 115, C10015, doi:10.1029/2009JC005387, 2010.

Arctic plankton modeling

V. Le Fouest et al.

Title Page

Abstract | Introduction

Conclusions | References

Tables | Figures

◄ | ►

◄ | ►

Back | Close

Full Screen / Esc

Printer-friendly Version

Interactive Discussion

Table 1. Differential equations for the 10-component plankton ecosystem model: nitrate (NO_3), ammonium (NH_4), large and small phytoplankton (LP and SP, respectively), large and small zooplankton (LZ and SZ, respectively), bacteria (BACT), particulate organic nitrogen (PON), labile and refractory dissolved organic nitrogen (DONl and DONp, respectively).

$$\frac{\partial NO_3}{\partial t} = \nabla\left(K_z \nabla NO_3\right) + \text{nitrif} - \lim_{NO_3}^{LP}\mu_{LP}LP - \lim_{NO_3}^{SP}\mu_{SP}SP$$

$$\frac{\partial NH_4}{\partial t} = \nabla\left(K_z \nabla NH_4\right) - \lim_{NH_4}^{LP}\mu_{LP}LP - \lim_{NH_4}^{SP}\mu_{SP}SP - \text{nitrif} - \text{Ubact}_{NH_4}\text{BACT} + \text{ex}_{BACT}$$
$$+ \text{ex}_{SZ}(1 - \text{assim}_{SZ})G_{SZ}SZ + \text{ex}_{LZ}LZ + \text{ammo}$$

$$\frac{\partial LP}{\partial t} = \nabla\left(K_z \nabla LP\right) + \mu_{LP}LP - G_{LZ}\text{pf}_{LP}LZ - m_{LP}LP + \frac{\partial}{\partial z}(\text{sedlpLP})$$

$$\frac{\partial SP}{\partial t} = \nabla\left(K_z \nabla SP\right) + \mu_{SP}SP - G_{SZ}\text{pf}_{SP}SZ - m_{SP}SP$$

$$\frac{\partial LZ}{\partial t} = \nabla\left(K_z \nabla LZ\right) + \text{assim}_{LZ}G_{LZ}LZ - m_{LZ}LZ^2 - \text{ex}_{LZ}LZ$$

$$\frac{\partial SZ}{\partial t} = \nabla\left(K_z \nabla SZ\right) + \text{assim}_{SZ}G_{SZ}SZ - m_{SZ}SZ^2 - G_{LZ}(1 - \text{pf}_{LP})LZ$$

$$\frac{\partial BACT}{\partial t} = \nabla\left(K_z \nabla BACT\right) + \text{Ubact}_{NH_4}\text{BACT} + \text{Ubact}_{DONl}\text{BACT} - \text{ex}_{BACT} - G_{SZ}(1 - \text{pf}_{SP})SZ$$

$$\frac{\partial PON}{\partial t} = \nabla\left(K_z \nabla PON\right) + (1 - \text{assim}_{LZ})G_{LZ}LZ + m_{LZ}LZ^2 + m_{LP}LP + \frac{\partial}{\partial z}(\text{sedponPON}) - \text{fgPON}$$

$$\frac{\partial DONl}{\partial t} = \nabla\left(K_z \nabla DONl\right) + \text{fgPON} + m_{SZ}SZ^2 + m_{SP}SP + (1 - \text{ex}_{SZ})(1 - \text{assim}_{SZ})G_{SZ}SZ - \text{Ubact}_{DONl}\text{BACT}$$

$$\frac{\partial DONp}{\partial t} = \nabla\left(K_z \nabla DONp\right) - \text{ammo}$$

Table 2. Model parameters.

Symbol	Description	Value	Units
kw	Light attenuation coefficient due to water	0.04	m^{-1}
knonchl	Light attenuation coefficient due to nonchlorophyllous matter	0.05	m^{-1}
$K_{NO_3}^{LP}$	Half-saturation constant for NO_3 use by LP	1	$mmol\,N\,m^{-3}$
$K_{NO_3}^{SP}$	Half-saturation constant for NO_3 use by SP	0.5	$mmol\,N\,m^{-3}$
$K_{NH_4}^{LP}$	Half-saturation constant for NH_4 use by LP	20	$mmol\,N\,m^{-3}$
$K_{NH_4}^{SP}$	Half-saturation constant for NH_4 use by SP	0.1	$mmol\,N\,m^{-3}$
K_E^{LP}	Photoacclimation parameter	8	$Ein\,m^{-2}\,d^{-1}$
K_E^{SP}	Photoacclimation parameter	4	$Ein\,m^{-2}\,d^{-1}$
$\left(\frac{Chl}{C}\right)_{max}^{LP}$	Maximum Chl to C ratio for LP	0.0125	$g\,g^{-1}$
$\left(\frac{Chl}{C}\right)_{max}^{SP}$	Maximum Chl to C ratio for LP	0.02	$g\,g^{-1}$
μ_{max}^{LP}	Maximum growth rate for LP	1.2	d^{-1}
μ_{max}^{SP}	Maximum growth rate for SP	0.9	d^{-1}
sed_lp	LP sinking rate	0.1	m^{-1}
m_{LP}	LP basal mortality	0.005	d^{-1}
m_{SP}	SP basal mortality	0.005	d^{-1}
G_{LZ}^{max}	Maximum grazing rate for LZ	0.3	d^{-1}
λ	Ivlev constant for LZ	0.5	$(mmol\,N\,m^{-3})^{-1}$
G_{SZ}^{max}	Maximum grazing rate for SZ	1	d^{-1}
K_G	Half-saturation constant for SZ grazing	0.8	$mmol\,N\,m^{-3}$
$assim_{LZ}$	LZ assimilation	0.7	%
$assim_{SZ}$	SZ assimilation	0.3	%
ex_{SZ}	DONI egestion by SZ	0.4	%
ex_{LZ}	NH_4 excretion by LZ	0.01	d^{-1}
m_{LZ}	LZ mortality	0.2	$(mmol\,N\,m^{-3})^{-1}$
m_{LZ}	LZ mortality	0.05	$(mmol\,N\,m^{-3})^{-1}$
$Ubact_{max}$	BACT maximum growth rate	2	d^{-1}
$K_{NH_4}^{BACT}$	Half-saturation constant for NH_4 use by BACT	0.1	$mmol\,N\,m^{-3}$
K_{DONI}^{BACT}	Half-saturation constant for DONI use by BACT	0.1	$mmol\,N\,m^{-3}$
ex_{BACT}	NH_4 release by bacteria	0.05	%
sed_pon	PON sinking rate	100	$m\,d^{-1}\,(mmol\,N\,m^{-3})^{-1}$
fg	PON fragmentation	0.05	d^{-1}
$nitrif_{max}$	Maximum NH_4 nitrification rate	0.05	d^{-1}
K_{nitrif}^N	Half-saturation constant for NH_4 nitrification	0.07	$mmol\,N\,m^{-3}$
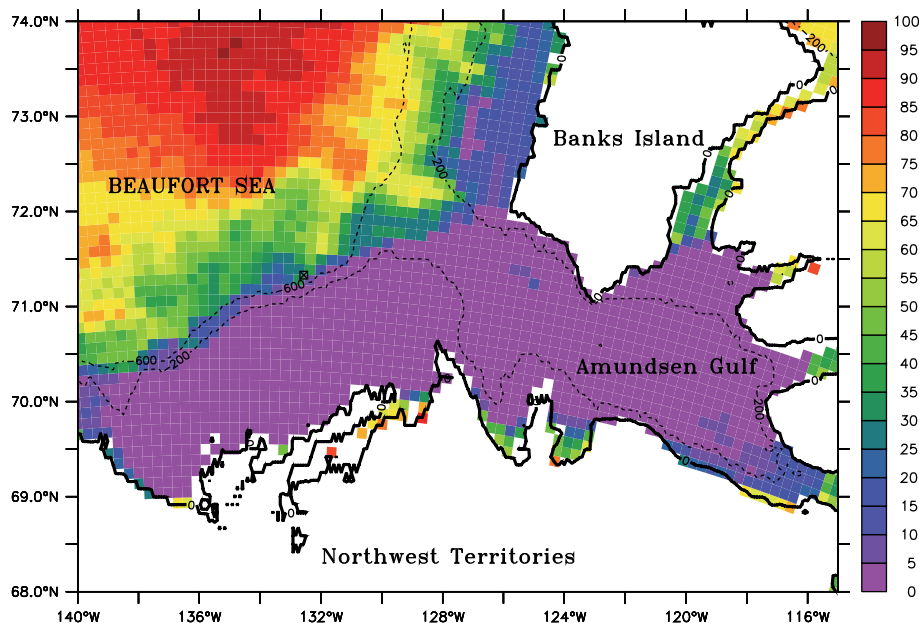
**Fig. 1.** Mean remotely-sensed sea ice concentration (%; calculated from Special Sensor Microwave Imager (SSM/I) data from http://cersat.ifremer.fr) for the 14–16 August 2009 sampling period. Station 345 is indicated by a black crossed square. The full and dashed black lines indicate the land contour and the 200 m and 600 m isobaths, respectively. Land appears in white.

Title Page

Abstract | Introduction

Conclusions | References

Tables | Figures

|◄ | ►|

◄ | ►

Back | Close

Full Screen / Esc

Printer-friendly Version

Interactive Discussion
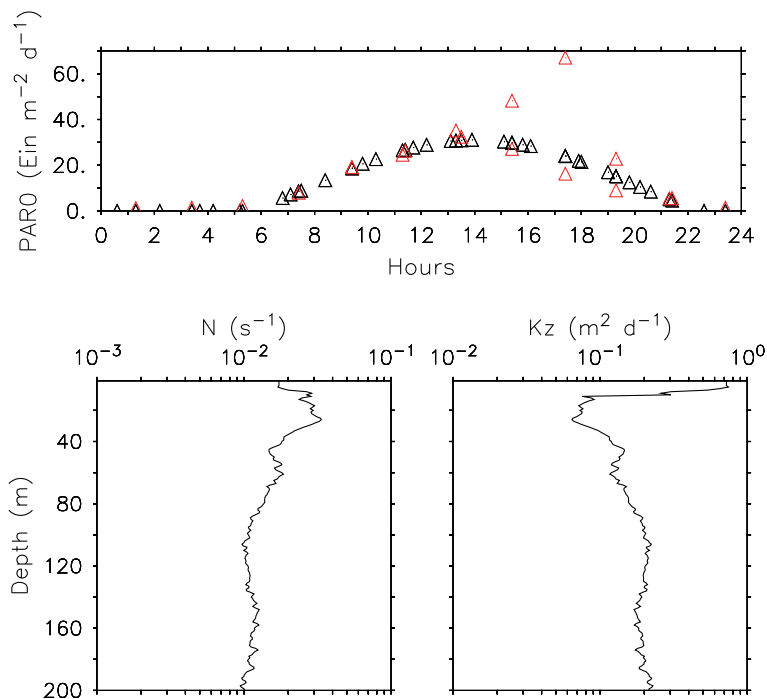
Fig. 2. Measured (14–15 August 2009, red triangles) and fitted from data (black triangles) surface PAR (PAR0, upper panel), 4-day (14–16 August 2009) averaged profile of measured Brunt-Väisälä frequency (N, lower left panel) and derived profile of eddy diffusion coefficient (K_z, lower right panel).
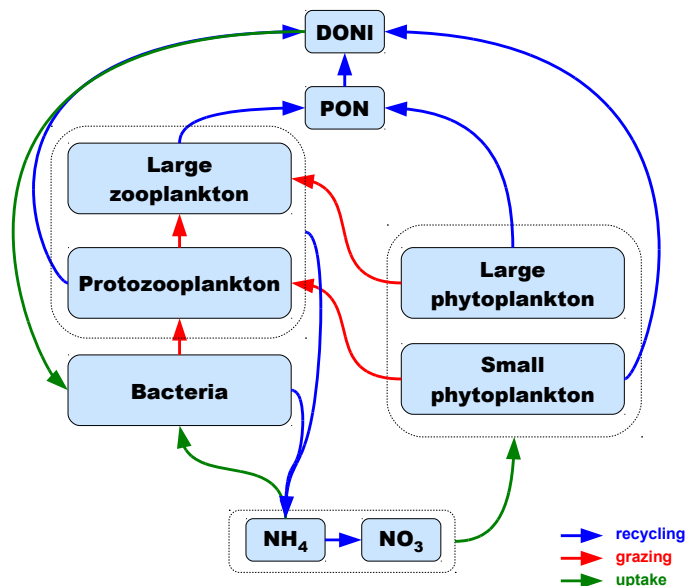
Fig. 3. Conceptual diagram of the plankton ecosystem model. The 10 state variables are nitrate (NO_3), ammonium (NH_4), Large ($> 5\,\mu m$) and small ($< 5\,\mu m$) phytoplankton, copepods, proto-zooplankton, bacteria, and detrital particulate and dissolved organic nitrogen (PON and DONI, respectively). Green, red and blue arrows represent nutrients uptake, grazing and nitrogen recycling, respectively.
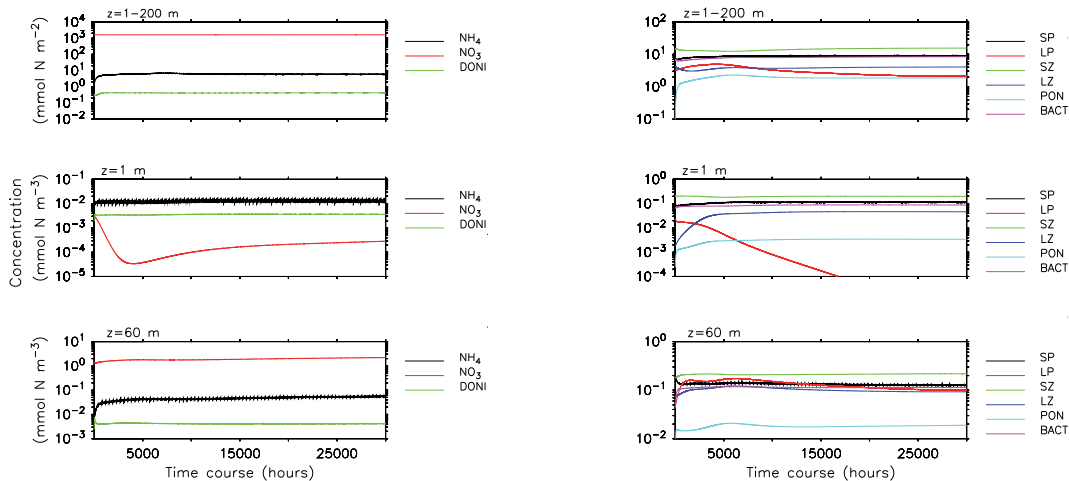
Fig. 4. Time course of the model state variables in the dissolved (left panels) and particulate (right panels) form integrated over the numerical domain (upper panels), at the surface (middle panels) and within the DCM.
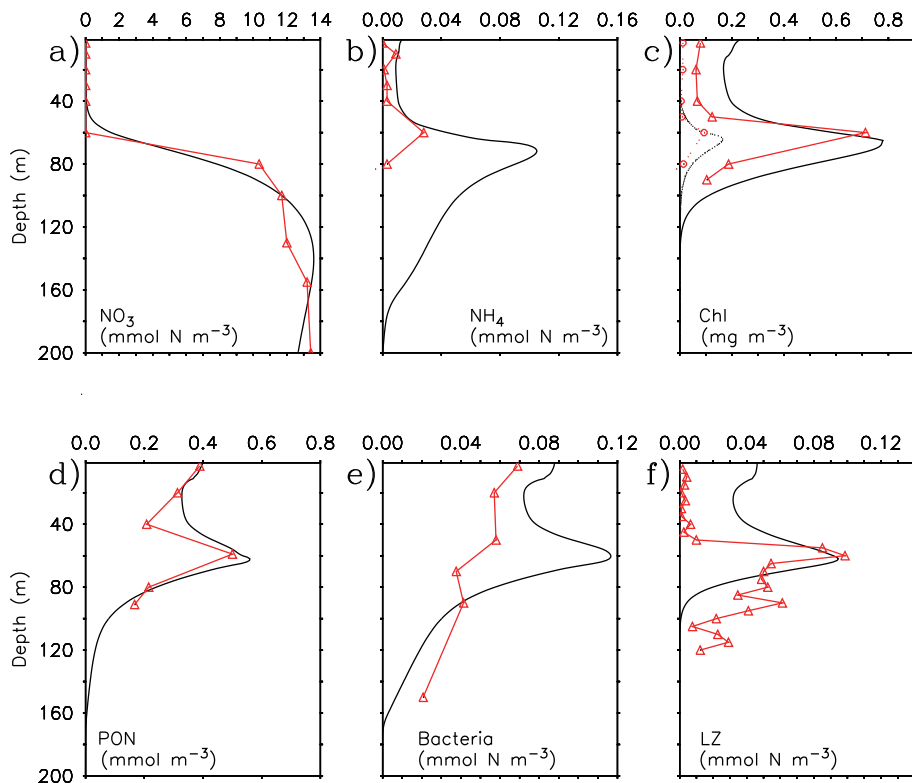
**Fig. 5.** Model-data comparisons (scalars) for the "standard" run. Model outputs are in black and observations in red: **(a)** NO_3, **(b)** NH_4, **(c)** Chl for SP and LP (in the model, full and dashed lines, respectively; in observations, triangles and circles, respectively), **(d)** total PON (i.e. sum of LP, SP, SZ, BACT and detrital PON in the model), **(e)** biomass of bacteria and **(f)** LZ.
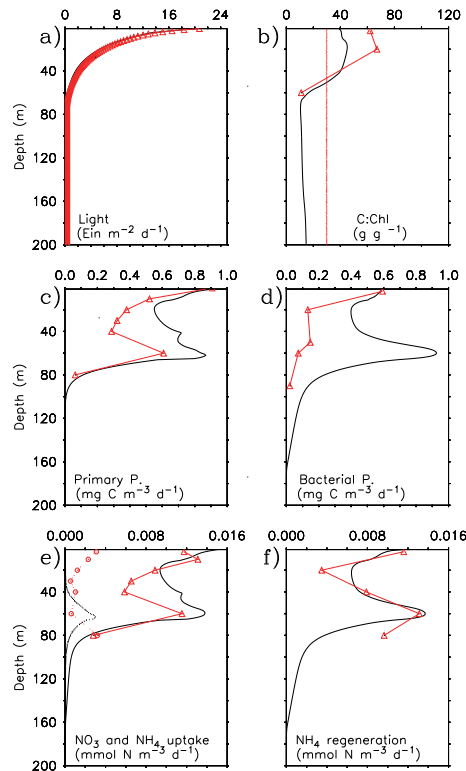
Fig. 6. Model-data comparisons (rates) for the "standard" run. Model outputs are in black and observations in red: **(a)** downwelling PAR, **(b)** C : Chl ratio (for SP in the model; for the observations derived from Claustre et al. (1999) (see text for details); the vertical dashed line is the mean C : Chl ratio according to DuRand et al., 2002, and Sherr et al., 2003), **(c)** primary production, **(d)** bacterial production, **(e)** NH_4 and NO_3 uptake (in the model, full and dashed lines, respectively; in the observations, triangles and circles, respectively) and **(f)** NH_4 regeneration.
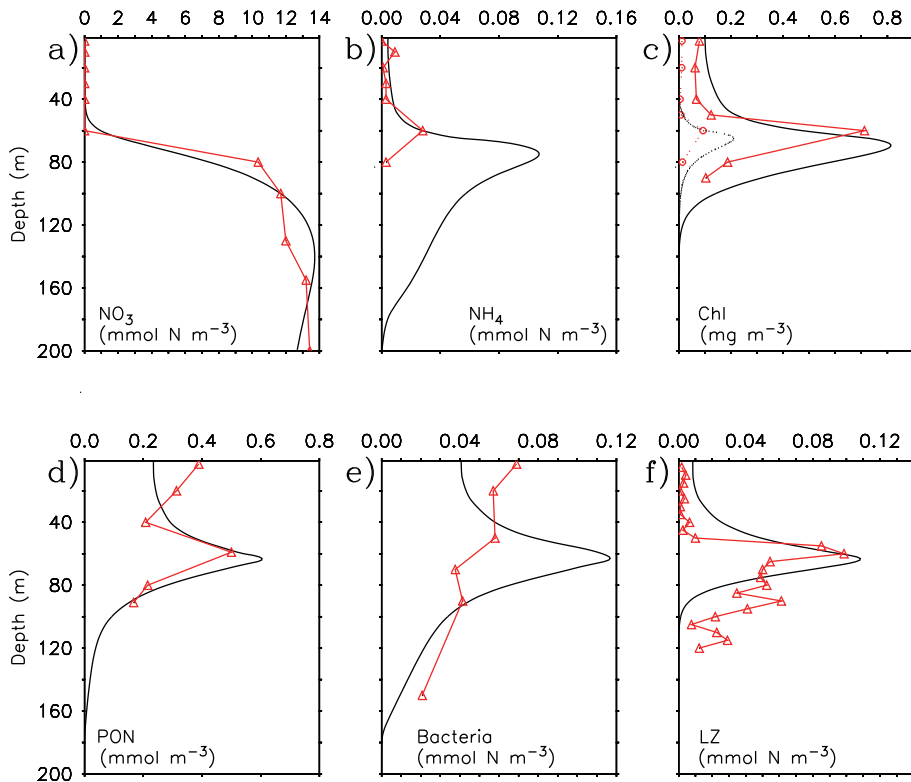
Fig. 7. Model-data comparisons (scalars) for the "no photoammonification" run. Model outputs are in black and observations in red: **(a)** NO$_3$, **(b)** NH$_4$, **(c)** Chl for SP and LP (in the model, full and dashed lines, respectively; in observations, triangles and circles, respectively), **(d)** total PON (i.e. sum of LP, SP, SZ, BACT and detrital PON in the model), **(e)** biomass of bacteria and **(f)** LZ.
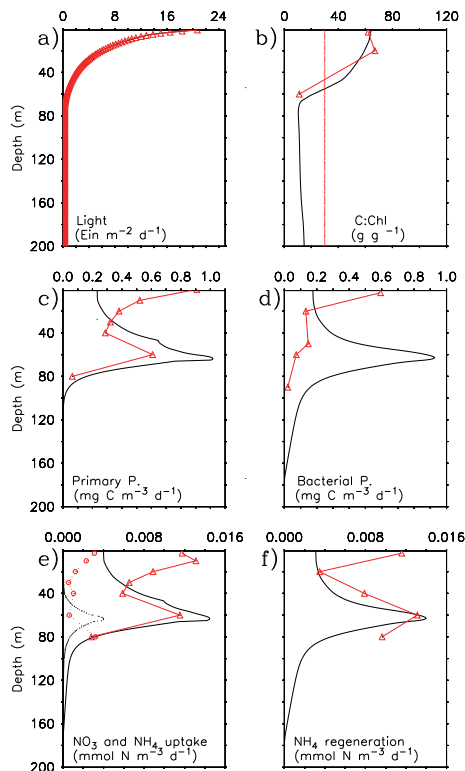
Fig. 8. Model-data comparisons (rates) for the "no photoammonification" run. Model outputs are in black and observations in red: **(a)** downwelling PAR, **(b)** C : Chl ratio (for SP in the model; for the observations derived from Claustre et al., 1999 (see text for details); the vertical dashed line is the mean C : Chl ratio according to DuRand et al., 2002, and Sherr et al., 2003), **(c)** primary production, **(d)** bacterial production, **(e)** NH_4 and NO_3 uptake (in the model, full and dashed lines, respectively; in the observations, triangles and circles, respectively) and **(f)** NH_4 regeneration.
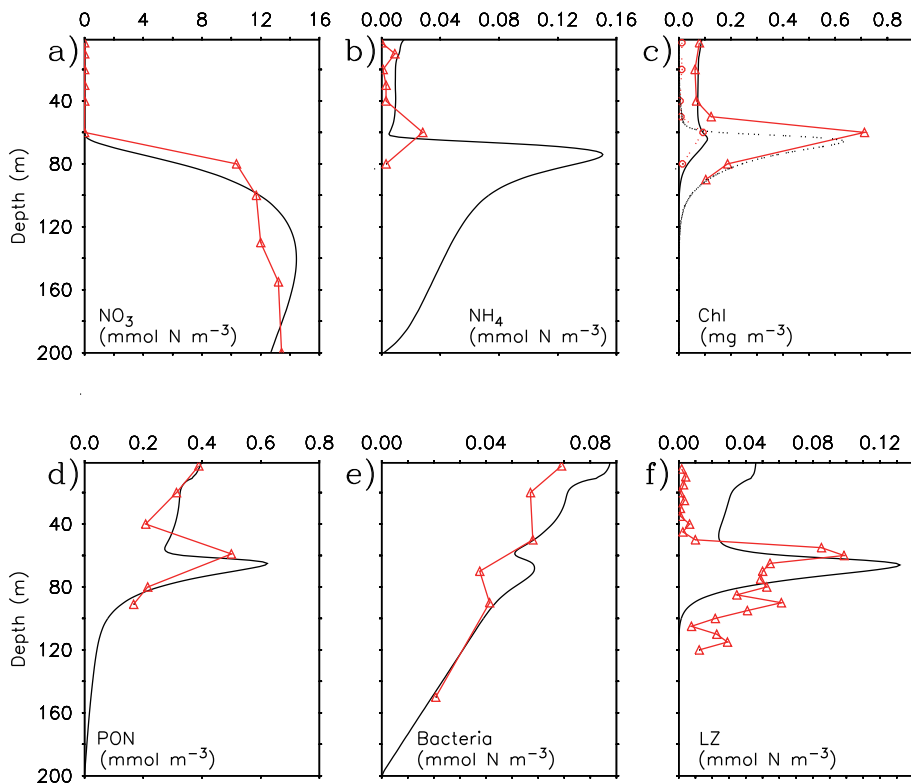
Fig. 9. Model-data comparisons (scalars) for the "constant C : Chl" run. Model outputs are in black and observations in red: **(a)** NO_3, **(b)** NH_4, **(c)** Chl for SP and LP (in the model, full and dashed lines, respectively; in observations, triangles and circles, respectively), **(d)** total PON (i.e. sum of LP, SP, SZ, BACT and detrital PON in the model), **(e)** biomass of bacteria and **(f)** LZ.
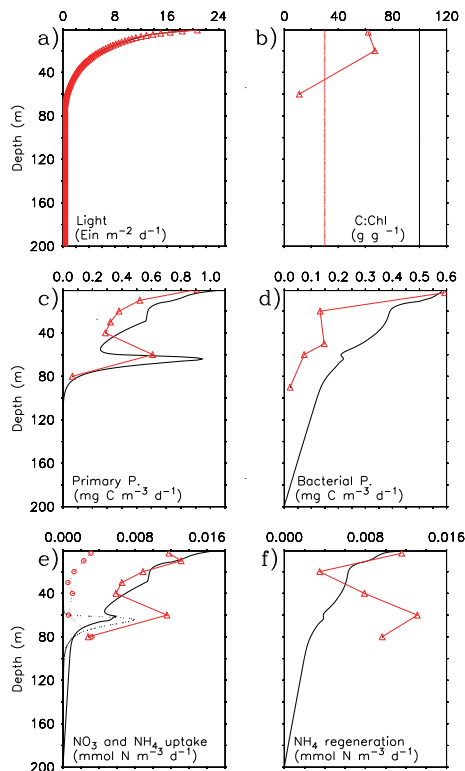
Fig. 10. Model-data comparisons (rates) for the "constant C : Chl" run. Model outputs are in black and observations in red: **(a)** downwelling PAR, **(b)** C : Chl ratio (for SP in the model; for the observations derived from Claustre et al., 1999 (see text for details); the vertical dashed line is the mean C : Chl ratio according to DuRand et al., 2002, and Sherr et al., 2003), **(c)** primary production, **(d)** bacterial production, **(e)** NH_4 and NO_3 uptake (in the model, full and dashed lines, respectively; in the observations, triangles and circles, respectively) and **(f)** NH_4 regeneration.

Title Page

Abstract | Introduction

Conclusions | References

Tables | Figures

◄ | ►

◄ | ►

Back | Close

Full Screen / Esc

Printer-friendly Version

Interactive Discussion